COMPUTATIONAL METHODS IN APPLIED MATHEMATICS, Vol.2(2002), No.3, pp.283–294

SOLUTION OF THE MULTI-INTERFACE STEFAN PROBLEM BY THE METHOD OF DYNAMIC ADAPTATION

VLADIMIR MAZHUKIN

Institute of Mathematical Modelling, Russian Academy of Science
4-A Miusskaya Sq., 124047 Moscow
E-mail: immras@orc.ru

MICHAIL CHUIKO

Institute of Mathematics, NAS of Belarus
11 Surganov Str., 220072 Minsk, Belarus
E-mail: chuiko@im.bas-net.by

Abstract — The application of the dynamic adaptation method to the numerical solution of multidimensional Stefan problems with explicit tracking of interfaces is considered. The dynamic adaptation method is based on the idea of transition to any non-stationary coordinate system. The results of the numerical experiment on modelling the pulsed action of high-energy fluxes on metals are presented.

2000 Mathematics Subject Classification: 65M06; 80A22; 65M50.

Keywords: Stefan problem, dynamic adaptation method, nonuniform grids, arbitrary domain.

1. Introduction

The interest in the Stefan problems is due to their important physical and technological applications in the cases of the action of concentrated energy fluxes on metals and ceramics. The processes of material processing by means of intense energy fluxes (laser radiation, electron and ion beams) are the basis for many technological operations like cutting, drilling, surface modification, and dimensional processing of condensed media [4,7]. The necessity for clear understanding of the above processes stimulates fundamental researches on the kinetics of fast phase transformations [8]. But theoretical investigations are especially urgent in the consideration of pulsed regimes of processing.

The main complexity of mathematical studies of Stefan-like problems is due to the presence of moving boundaries leading to essential nonlinearity. Analytical solutions of such problems can be obtained only under strong simplifying assumptions. There are two widely used approaches to the numerical solution: explicit tracking of moving surfaces [1,3] and use of smoothing procedures [6,10]. In the problem of the pulsed action of high-energy fluxes on materials, where the nonequilibrium of fast phase transformation can play a dominant role,

it is necessary to explicitly locate the phase boundaries and take into account the related processes.

In the present work, the application of the dynamic adaptation method [9] to the solution of a multi-interface Stefan problem in arbitrary two-dimensional areas with explicit tracking of the interfaces is considered. This method is widely used for solving one-dimensional problems of mathematical physics [2]. The dynamic adaptation method for solving two-dimensional problems is based on the idea of the transition, by means of the desired solution, to a non-stationary curvilinear coordinate system. The transition to a moving curvilinear coordinate system allows to eliminate problems related to moving boundaries. In this case, it is necessary to determine not only the values of the unknown functions but also the coordinates of grid points. The movement of grid points is described by partial differential equations added to the problem. In this coordinate system with fixed boundaries, the problem is described by an extended system of differential equations, one part of which describes the physical phenomenon and second one concerns the movement of the grid points.

The results of the computing experiment on the solution of a problem typical of the material processing by intense energy fluxes are presented. The main features of such problems are the presence of melting-crystallization and evaporation processes and a significant difference in sizes between the target and the energy release zone.

2. Mathematical model

The mathematical formulation of the classical version of the two-dimensional Stefan problem describing the melting and crystallization processes of pure materials is reduced to the quasi-linear heat transfer equation in an arbitrary region Ω_{xy} with an a priori unknown moving boundary $\Gamma_{sl}(t)$ which separates the solid $\Omega_s(t)$ and liquid $\Omega_l(t)$ phases:

$$\left[\frac{\partial H}{\partial t} = -\frac{\partial W_1}{\partial x} - \frac{\partial W_2}{\partial y} + g\right]_m, \quad m = s, l, \tag{2.1}$$

$$H_m = c_p \rho_m T, \quad \left(W_1\right)_m = -\lambda_m(T)\frac{\partial T}{\partial x}, \quad \left(W_2\right)_m = -\lambda_m(T)\frac{\partial T}{\partial y}.$$

At $\Gamma_{sl}(t)$ the differential Stefan condition

$$W_l^n - W_s^n = L_m \rho v_{sl}^n, \quad W_s^\tau = W_l^\tau \tag{2.2}$$

is fulfilled and the temperature is continuous and equal to the equilibrium transition temperature

$$T_s = T_l = T_m. \tag{2.3}$$

Here superscripts n and τ indicate normal and tangent components, subscripts s and l refer to solid and liquid phases, T_m, L_m are the temperature and the latent heat of melting/crystallization, v_{sl} is the velocity of motion of the interface. At the domain boundary $\partial\Omega_{xy}$ the boundary conditions are specified in the form

$$(\vec{W}, \vec{n})|_{\partial\Omega_{xy}} = f,$$

where $\vec{W} = (W_1, W_2)$ is the vector of the heat flow, $\vec{n}$ is the external normal to $\partial\Omega_{xy}$, f is the function specified at $\partial\Omega_{xy}$.

The account of the evaporation leads to appearance of the second mobile interface $\Gamma_{lv}(t)$ in area Ω_{xy}. The process of advanced surface evaporation at this boundary is described by three conservation laws (mass, momentum and energy)

$$\rho_l v_{lv}^n = \rho_v(u - v_{lv}^n), \tag{2.4}$$

$$P_l + \rho_l(v_{lv}^n)^2 = P_v + \rho_v(u - v_{lv}^n)^2, \tag{2.5}$$

$$-\lambda\frac{\partial T}{\partial n} = G^n - L_v\rho_l v_{lv}^n \tag{2.6}$$

and two additional relations describing the kinetics of phase transformations that are determined from the Knudsen layer approximation [5]

$$T_v = T_v(T_l, M), \quad \rho_v = \rho_v(\rho_{sat}, M),$$

where the index v denotes vapor, G is the energy source intensity, u is the gas-dynamic velocity, v_{lv}^n is the velocity of the evaporation front, L_v is the evaporation heat, P_v is the pressure, M is the Mach number, and ρ_{sat} denotes the saturated vapor density. For $M = 0$ these relations take the following form: $T_v = 0.633T_l$, $\rho_v = 0.326\rho_{sat}$. The value of ρ_{sat} is determined from the equation of state $\rho_{sat} = P_{sat}/(RT_l)$, where $P_{sat} = P_0\exp\Big(\frac{L_v}{R}\Big(\frac{1}{T_b} - \frac{1}{T_b}\Big)\Big)$. Here P_{sat} is the saturated vapor pressure, P_0 is the atmospheric pressure, T_b is the boiling temperature, and R is the gas constant.

3. Problem statement in an arbitrary curvilinear unsteady coordinate system

The solution of this problem consists of the determination of the temperature fields and position of phase fronts $\Gamma_{sl}(t)$, $\Gamma_{lv}(t)$. To numerically solve of multidimensional boundary problems on arbitrarily shaped regions, it is convenient to use boundary fitted curvilinear coordinates. To map the physical space with coordinates (x, y, t) onto a computational one with (ξ, η, τ), we use the general transformation $\xi = \xi(x, y, t)$, $\eta = \eta(x, y, t)$, $\tau = t$. The differential problem (2.1) - (2.6) in the arbitrary non-stationary curvilinear coordinate system (ξ, η, τ) can be written in the form:

$$\begin{aligned}\Big[\frac{\partial}{\partial\tau}(\psi H) = &-\frac{\partial}{\partial\xi}\Big[(\rho W_1 + HQ_1)\frac{\partial y}{\partial\eta} - (\rho W_2 + HQ_2)\frac{\partial x}{\partial\eta}\Big] \\ &- \frac{\partial}{\partial\eta}\Big[-(\rho W_1 + HQ_1)\frac{\partial y}{\partial\xi} + (\rho W_2 + HQ_2)\frac{\partial x}{\partial\xi}\Big] + \psi g\Big]_m,\end{aligned} \tag{3.1}$$

$$\Big[\frac{\partial x}{\partial\tau} = -\frac{Q_1}{\rho}\Big]_m, \quad \Big[\frac{\partial y}{\partial\tau} = -\frac{Q_2}{\rho}\Big]_m, \quad m = s, l \tag{3.2}$$

with the corresponding boundary conditions on the lines of the phase transitions $(\xi, \eta = \eta_{sl}) \in \Gamma_{sl}$:

$$\Big[\Big(-W_1\frac{\partial y}{\partial\xi} + W_2\frac{\partial x}{\partial\xi}\Big)_l - \Big(-W_1\frac{\partial y}{\partial\xi} + W_2\frac{\partial x}{\partial\xi}\Big)_s\Big]\gamma^{\frac{1}{2}} = -L_m Q_{sl}^n, \tag{3.3}$$

$(\xi,\eta) \in \Gamma_{lv}$:

$$Q^n_{lv} = -\rho_v\Big(u + \frac{Q^n_{lv}}{\rho_l}\Big), \tag{3.4}$$

$$P_l + \frac{(Q^n_{lv})^2}{\rho_l} = P_v + \rho_v\Big(u + \frac{Q^n_{lv}}{\rho_l}\Big)^2, \tag{3.5}$$

$$\Big(-W_1\frac{\partial y}{\partial \xi} + W_2\frac{\partial x}{\partial \xi}\Big)_l \gamma^{\frac{1}{2}} = G^n + L_v Q^n_{lv}, \quad \eta = const, \tag{3.6}$$

$$\Big(W_1\frac{\partial y}{\partial \eta} - W_2\frac{\partial x}{\partial \eta}\Big)_l \alpha^{\frac{1}{2}} = G^n + L_v Q^n_{lv}, \quad \xi = const, \tag{3.7}$$

where

$$W_1 = -\frac{\lambda\rho}{\psi}\left(\frac{\partial y}{\partial \eta}\frac{\partial T}{\partial \xi} - \frac{\partial y}{\partial \xi}\frac{\partial T}{\partial \eta}\right), \quad W_2 = -\frac{\lambda\rho}{\psi}\left(-\frac{\partial x}{\partial \eta}\frac{\partial T}{\partial \xi} + \frac{\partial x}{\partial \xi}\frac{\partial T}{\partial \eta}\right),$$

$$\psi = \rho J^{-1} = \rho\left(\frac{\partial x}{\partial \xi}\frac{\partial y}{\partial \eta} - \frac{\partial x}{\partial \eta}\frac{\partial y}{\partial \xi}\right), \qquad \alpha = \left(\frac{\partial x}{\partial \eta}\right)^2 + \left(\frac{\partial y}{\partial \eta}\right)^2, \quad \gamma = \left(\frac{\partial x}{\partial \xi}\right)^2 + \left(\frac{\partial y}{\partial \xi}\right)^2.$$

Here Q_{sl} and Q_{lv} are the flows of substance through the interfaces Γ_{sl} and Γ_{lv} respectively, Q_1, Q_2 are the arbitrary transformation functions and J^{-1} is the Jacobian of inverse transformation.

4. Algorithm of solution

For the finite difference approximation of (3.1) - (3.7) in the $\Omega_{\xi\eta} \times [0, t_0]$ domain of the generalized coordinates ξ, η, τ, where $\Omega_{\xi\eta} = \{(\xi,\eta) : 0 \leqslant \xi \leqslant 1,\ 0 \leqslant \eta \leqslant 1\}$ is the rectangle, we introduce the rectangular grid ω with steps h_ξ, h_η, $\Delta\tau^j$ respectively.

The functions $x^j_{i,k}$, $y^j_{i,k}$, $Q^j_{1,i,k}$, $Q^j_{2,i,k}$ are determined in the grid nodes, while the functions $T^j_{i+1/2,k+1/2}$, $\psi^j_{i+1/2,k+1/2}$, $H^j_{1,i+1/2,k+1/2}$ are evaluated at the cell centers. Variables $W^j_{1,i+1/2,k}$, $W^j_{2,i+1/2,k}$, $W^j_{1,i,k+1/2}$, $W^j_{2,i,k+1/2}$ are evaluated at the centers of the cell edges. Using the integro-interpolational method [11], the initial differential problem is approximated by the implicit difference scheme

$$\begin{aligned}
\frac{(\psi H)^{j+1}_{i+1/2,k+1/2} - (\psi H)^j_{i+1/2,k+1/2}}{\Delta\tau^j} = -\frac{1}{h_\xi h_\eta}\Big\{&(\rho W_1 + HQ_1)_{i+1,k+1/2}\,(y_{i+1,k+1} - y_{i+1,k}) \\
&- (\rho W_1 + HQ_1)_{i,k+1/2}\,(y_{i,k+1} - y_{i,k}) - (\rho W_1 + HQ_1)_{i+1/2,k+1}\,(y_{i+1,k+1} - y_{i,k+1}) \\
&+ (\rho W_1 + HQ_1)_{i+1/2,k}\,(y_{i+1,k} - y_{i,k}) - (\rho W_2 + HQ_2)_{i+1,k+1/2}\,(x_{i+1,k+1} - x_{i+1,k}) \\
&- (\rho W_2 + HQ_2)_{i,k+1/2}\,(x_{i,k+1} - x_{i,k}) - (\rho W_2 + HQ_2)_{i+1/2,k+1}\,(x_{i+1,k+1} - x_{i,k+1}) \\
&+ (\rho W_2 + HQ_2)_{i+1/2,k}\,(x_{i+1,k} - x_{i,k})\Big\}^{j+1} - (\psi g)^{j+1}_{i+1/2,k+1/2}.
\end{aligned}$$

Here

$$W_{1,i+1/2,k} = -\frac{\lambda\rho}{\psi_{i+1/2,k}h_\xi h_\eta}\left\{\left(y_{i+1/2,k+1/2} - y_{i+1/2,k-1/2}\right)\left(T_{i+1,k} - T_{i,k}\right)\right.$$
$$\left. - \left(y_{i+1,k} - y_{i,k}\right)\left(T_{i+1/2,k+1/2} - T_{i+1/2,k-1/2}\right)\right\},$$
$$W_{1,i,k+1/2} = -\frac{\lambda\rho}{\psi_{i,k+1/2}h_\xi h_\eta}\left\{\left(y_{i,k+1} - y_{i,k}\right)\left(T_{i+1/2,k+1/2} - T_{i-1/2,k+1/2}\right)\right.$$
$$\left. - \left(y_{i+1/2,k+1/2} - y_{i-1/2,k+1/2}\right)\left(T_{i,k+1} - T_{i,k}\right)\right\},$$
$$W_{2,i+1/2,k} = -\frac{\lambda\rho}{\psi_{i+1/2,k}h_\xi h_\eta}\left\{-\left(x_{i+1/2,k+1/2} - x_{i+1/2,k-1/2}\right)\left(T_{i+1,k} - T_{i,k}\right)\right.$$
$$\left. + \left(x_{i+1,k} - x_{i,k}\right)\left(T_{i+1/2,k+1/2} - T_{i+1/2,k-1/2}\right)\right\},$$
$$W_{2,i,k+1/2} = -\frac{\lambda\rho}{\psi_{i,k+1/2}h_\xi h_\eta}\left\{-\left(x_{i,k+1} - x_{i,k}\right)\left(T_{i+1/2,k+1/2} - T_{i-1/2,k+1/2}\right)\right.$$
$$\left. + \left(x_{i+1/2,k+1/2} - x_{i-1/2,k+1/2}\right)\left(T_{i,k+1} - T_{i,k}\right)\right\}.$$

The required interpolations are performed by the following formulas:

$$H_{i,k+1/2} = 0.5(H_{i+1/2,k+1/2} + H_{i-1/2,k+1/2}),$$
$$H_{i+1/2,k} = 0.5(H_{i+1/2,k+1/2} + H_{i+1/2,k-1/2}),$$
$$Q_{i,k+1/2} = 0.5(Q_{i,k+1} + Q_{i,k}), \quad Q_{i+1/2,k} = 0.5(Q_{i+1,k} + Q_{i,k}),$$
$$x_{i+1/2,k+1/2} = 0.25(x_{i,k} + x_{i,k+1} + x_{i+1,k} + x_{i+1,k+1}),$$
$$y_{i+1/2,k+1/2} = 0.25(y_{i,k} + y_{i,k+1} + y_{i+1,k} + y_{i+1,k+1}).$$

To realize the difference scheme, algorithm based on two enclosed iteration cycles was used at each time step $\Delta\tau^j$. In the first cycle, the $Q_{i,k}$ velocities of the grid nodes and their position were determined and in the second cycle the temperature distribution in the domains Ω_l, Ω_s was calculated. The obtained systems of linear algebraic equations were solved by the method given in [12]. The value of the normal component of the mass flow on the line of the phase front Γ_{sl} in the edge centers of cells is determined from the Stefan condition:

$$Q^n_{i+1/2,k} = L_m^{-1}\left[(W^n_{i+1/2,k})_s - (W^n_{i+1/2,k})_l\right], \; i = 0, \ldots, I-1, \; k = k_{sl}.$$

Here $(\cdot)^n$ is the normal component of the corresponding vector with respect to the line of the phase front. The value of the normal component of the mass flow on the line Γ_{lv} is determined from the equation $Q^n_{i+1/2,1} = -\rho_l v^n_{lv,i+1/2,1}$, $i = 0, \ldots, I-1$. To determine the velocity components for the nodes of the phase front Γ_{sl}, the mass conservation law was used:

$$\left(x_{i,k} - x_{i-1/2,k}, y_{i,k} - y_{i-1/2,k}\right) \times \left(Q_{1,i-1/2,k}, Q_{2,i-1/2,k}\right)$$
$$= \left(x_{i,k} - \hat{x}_{i-1/2,k}, y_{i,k} - \hat{y}_{i-1/2,k}\right) \times \left(Q_{1,i,k}, Q_{2,i,k}\right),$$
$$\left(x_{i+1/2,k} - x_{i,k}, y_{i+1/2,k} - y_{i,k}\right) \times \left(Q_{1,i+1/2,k}, Q_{2,i+1/2,k}\right)$$
$$= \left(\hat{x}_{i+1/2,k} - x_{i,k}, \hat{y}_{i+1/2,k} - y_{i,k}\right) \times \left(Q_{1,i,k}, Q_{2,i,k}\right),$$
$$i = 1, 2, \ldots, I-1,$$
$$\left(x_{1/2,k} - x_{0,k}, y_{1/2,k} - y_{0,k}\right) \times \left(Q_{1,1/2,k}, Q_{2,1/2,k}\right)$$
$$= \left(\hat{x}_{1/2,k} - x_{0,k}, \hat{y}_{1/2,k} - y_{i,k}\right) \times \left(Q_{1,i,k}, Q_{2,i,k}\right),$$

$$\vec{n}\big|_{(x_{0,k},y_{0,k})} \cdot (Q_{1,0,k}, Q_{2,0,k}) = 0,$$

$$(x_{I,k} - x_{I-1/2,k}, y_{I,k} - y_{I-1/2,k}) \times (Q_{1,I-1/2,k}, Q_{2,I-1/2,k})$$

$$= (x_{I,k} - \hat{x}_{I-1/2,k}, y_{I,k} - \hat{y}_{I-1/2,k}) \times (Q_{1,I,k}, Q_{2,I,k}),$$

$$\vec{n}\big|_{(x_{I,k},y_{I,k})} \cdot (Q_{1,I,k}, Q_{2,I,k}) = 0,$$

where

$$\hat{x}_{i\pm1/2,k} = x_{i\pm1/2,k} - Q_{i\pm1/2,k}\Delta\tau^j/\rho, \quad \hat{y}_{i\pm1/2,k} = y_{i\pm1/2,k} - Q_{i\pm1/2,k}\Delta\tau^j/\rho.$$

Here $k = k_{sl}$, $\vec{a} \times \vec{b}$ is the vector product, $\vec{a} \cdot \vec{b}$ is the scalar product of vectors $\vec{a}$ and $\vec{b}$, $\vec{n}$ is the unit vector of the normal direction to the domain boundary $\partial\Omega_{xy}$. Similar equations were used to determine the mass flows in the nodes of the moving boundary Γ_{lv}.

For redistribution of the nodes within subregions Ω_s and Ω_l, the condition of quasi-uniform distribution was used:

$$\frac{\partial x}{\partial \tau} = \frac{D_\xi}{\alpha}\left[\left(\frac{\partial x}{\partial \xi}\right)^2 \frac{\partial^2 x}{\partial \xi^2} + \frac{\partial x}{\partial \xi}\frac{\partial y}{\partial \xi}\frac{\partial^2 y}{\partial \xi^2}\right] + \frac{D_\eta}{\gamma}\left[\left(\frac{\partial x}{\partial \eta}\right)^2 \frac{\partial^2 x}{\partial \eta^2} + \frac{\partial x}{\partial \eta}\frac{\partial y}{\partial \eta}\frac{\partial^2 y}{\partial \eta^2}\right],$$

$$\frac{\partial y}{\partial \tau} = \frac{D_\xi}{\alpha}\left[\left(\frac{\partial y}{\partial \xi}\right)^2 \frac{\partial^2 y}{\partial \xi^2} + \frac{\partial x}{\partial \xi}\frac{\partial y}{\partial \xi}\frac{\partial^2 x}{\partial \xi^2}\right] + \frac{D_\eta}{\gamma}\left[\left(\frac{\partial y}{\partial \eta}\right)^2 \frac{\partial^2 y}{\partial \eta^2} + \frac{\partial x}{\partial \eta}\frac{\partial y}{\partial \eta}\frac{\partial^2 x}{\partial \eta^2}\right].$$

Here D_ξ, D_η are the diffusion coefficients for the distribution of the computational grid nodes along the coordinate lines $\xi = \text{const}$ and $\eta = \text{const}$ respectively.

This system of differential equations is approximated by the implicit difference scheme with central differences. For this scheme realization the following iterative process was used:

$$x_\tau^{(s+1)} = \frac{D_\xi}{\alpha^{(s)}}\left[\left(x_{\mathring{\xi}}^{(s)}\right)^2 x_{\bar{\xi}\xi}^{(s+1)} + x_{\mathring{\xi}}^{(s)} y_{\mathring{\xi}}^{(s)} y_{\bar{\xi}\xi}^{(s)}\right] + \frac{D_\eta}{\gamma^{(s)}}\left[\left(x_{\mathring{\eta}}^{(s)}\right)^2 x_{\bar{\eta}\eta}^{(s+1)} + x_{\mathring{\eta}}^{(s)} y_{\mathring{\eta}}^{(s)} y_{\bar{\eta}\eta}^{(s)}\right],$$

$$y_\tau^{(s+1)} = \frac{D_\xi}{\alpha^{(s)}}\left[\left(y_{\mathring{\xi}}^{(s)}\right)^2 y_{\bar{\xi}\xi}^{(s+1)} + x_{\mathring{\xi}}^{(s)} y_{\mathring{\xi}}^{(s)} x_{\bar{\xi}\xi}^{(s)}\right] + \frac{D_\eta}{\gamma^{(s)}}\left[\left(y_{\mathring{\eta}}^{(s)}\right)^2 y_{\bar{\eta}\eta}^{(s+1)} + x_{\mathring{\eta}}^{(s)} y_{\mathring{\eta}}^{(s)} x_{\bar{\eta}\eta}^{(s)}\right], \quad s = 0, 1, \cdots.$$

5. Freezing model problem

Verification of the dynamic adaptation method was carried out on the problem given in [10]. The Stefan problem for the freezing process is considered in the rectangular domain Ω_{xy} : $(0 \leqslant x \leqslant 1,\ 0 \leqslant y \leqslant 0.5)$ with planar interface $\Gamma_{sl}(t)$ between $\Omega_s(t)$ and $\Omega_l(t)$ subdomains. The coordinate axes were chosen such that the moving phase boundary $\Gamma_{sl}(t)$ temperature remains parallel to itself without being parallel to any of the axes (Fig. 1).

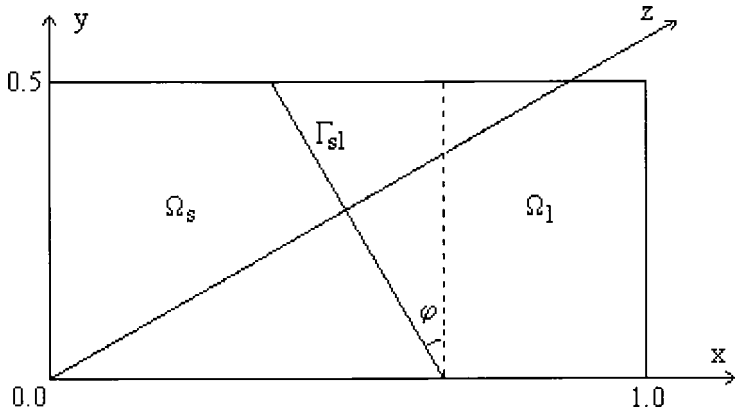

Figure 1. Initial domain for the freezing problem

The problem is described by the heat transfer equation (1) with constant coefficients. The following values of thermophysical parameters were used: $\lambda = c = \rho = 1$, $L_m = 1$, $T_m = 0$. By turning the original coordinate system at angle φ, the problem is reduced to the one-dimensional Stefan problem with the spatial coordinate $z = x\cos\varphi + y\sin\varphi$, which has a self-similar solution

$$T(z,t) = \begin{cases} -1 + \Phi\left(\frac{z}{2\sqrt{t}}\right)/\Phi(\beta), & 0 \leqslant z \leqslant z_\Gamma, \\ 0, & z > z_\Gamma, \end{cases}$$

where

$$\Phi(z) = \frac{2}{\sqrt{\pi}} \int_0^z e^{-y^2} dy, \quad z_\Gamma = 2\beta\sqrt{t}, \quad \beta = 0.6202.$$

A computational grid with total number of 11×6 nodes was used. The initial distribution was chosen to correspond to the self-similar solution at time $t_0 = 0.162$. The planar boundary is drawn at the angle $\varphi = 30°$. On passing to the curvilinear coordinate system (ξ, η, τ), the Ω_{xy} domain is mapped onto some rectangular domain $\Omega_{\xi\eta}$, in which the computational grid becomes equidistant in both directions. The planar boundary $\Gamma_{sl}(t)$ coincides with the coordinate line η_4, $k_{sl} = 4$ and its position remains unchanged with time (Fig. 2). The phase front position and the view of the computational grid in the physical space for different time moments are presented in Fig. 3.

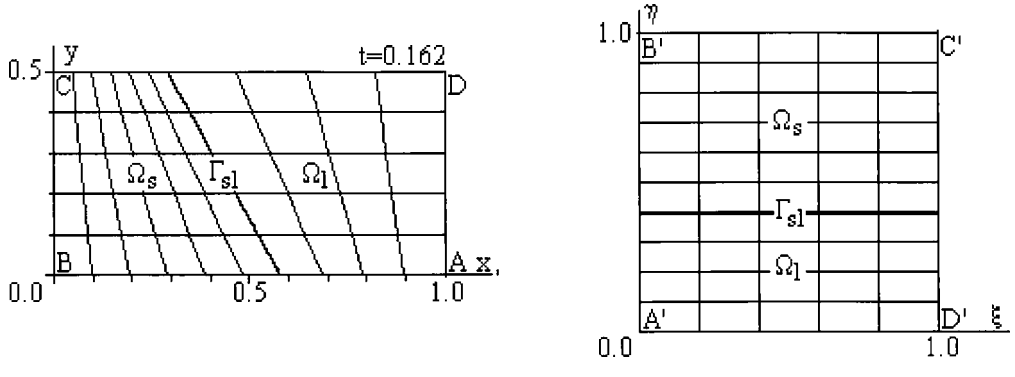

Figure 2. Mapping of the physical space onto the computational one for the freezing problem

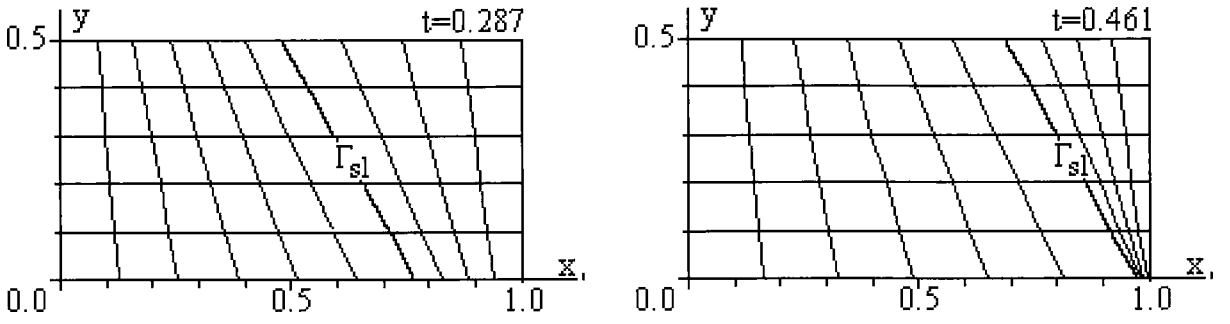

Figure 3. Phase boundary position versus the time for the freezing problem

The values of the absolute error $\Delta z_i = z_i - z_\Gamma$ and the relative error $\delta z_i = \Delta z_i / z_\Gamma$ in percent are presented in Table 1 which gives the deviation of the phase boundary from the planar one for different instants of time. Here z_Γ is the value of the coordinate z corresponding to the phase boundary, z_i is the calculated value of the coordinate z corresponding to the position of the i-th node at the phase boundary. The obtained results demonstrate a high accuracy of phase boundary tracking and validate the application of the adaptive grid with very small number of nodes, namely, about 30 in the Ω_s and Ω_l subdomains.

Table 1. Deviation of the phase boundary from the planar one

	$t = 0.2601, z(t) = 0.6326$			$t = 0.3363, z(t) = 0.7193$			$t = 0.4533, z(t) = 0.8351$		
i	z_i	Δz_i	δz_i	z_i	Δz_i	δz_i	z_i	Δz_i	δz_i
0	0.6337	$1.101 \cdot 10^{-3}$	0.1740	0.7203	$9.731 \cdot 10^{-4}$	0.1353	0.8362	$1.094 \cdot 10^{-3}$	0.1310
1	0.6340	$1.382 \cdot 10^{-3}$	0.2184	0.7210	$1.657 \cdot 10^{-3}$	0.2303	0.8363	$1.151 \cdot 10^{-3}$	0.1378
2	0.6337	$1.058 \cdot 10^{-3}$	0.1673	0.7212	$1.851 \cdot 10^{-3}$	0.2573	0.8385	$3.441 \cdot 10^{-3}$	0.4121
3	0.6330	$3.795 \cdot 10^{-4}$	0.0600	0.7197	$3.514 \cdot 10^{-4}$	0.0488	0.8350	$-5.612 \cdot 10^{-5}$	-0.0067
4	0.6339	$1.291 \cdot 10^{-3}$	0.2042	0.7211	$1.767 \cdot 10^{-3}$	0.2456	0.8374	$2.330 \cdot 10^{-3}$	0.2790
5	0.6342	$1.570 \cdot 10^{-3}$	0.2482	0.7211	$1.723 \cdot 10^{-3}$	0.2396	0.8370	$1.937 \cdot 10^{-3}$	0.2320

6. Numerical experiment

The proposed dynamic adaptation algorithm was used to solve the problem of the action of a high-energy flux on a metal target. A rectangular energy pulse of diameter $4 \cdot 10^{-2}$ cm and intensity 10^5 W/cm^2 influences on the surface of the triangle domain Ω_{xy}. The duration of processing is 0.3 s. The thermophysical parameters of aluminum were chosen.

The solution algorithm consists of two stages. At the first stage the entire domain is equal to the solid subdomain $\Omega_{xy} = \Omega_s$ and the process is described by the heat transfer equation. A fixed computational grid (21×21 nodes) with the maximum concentration of the nodes in the energy release zone had been constructed before the beginning of calculations (Fig. 4) by using the elliptic grid generator [13]. This grid was used for calculating the temperature field until the $T_{max} < T_m$ condition was fulfilled on the irradiated surface.

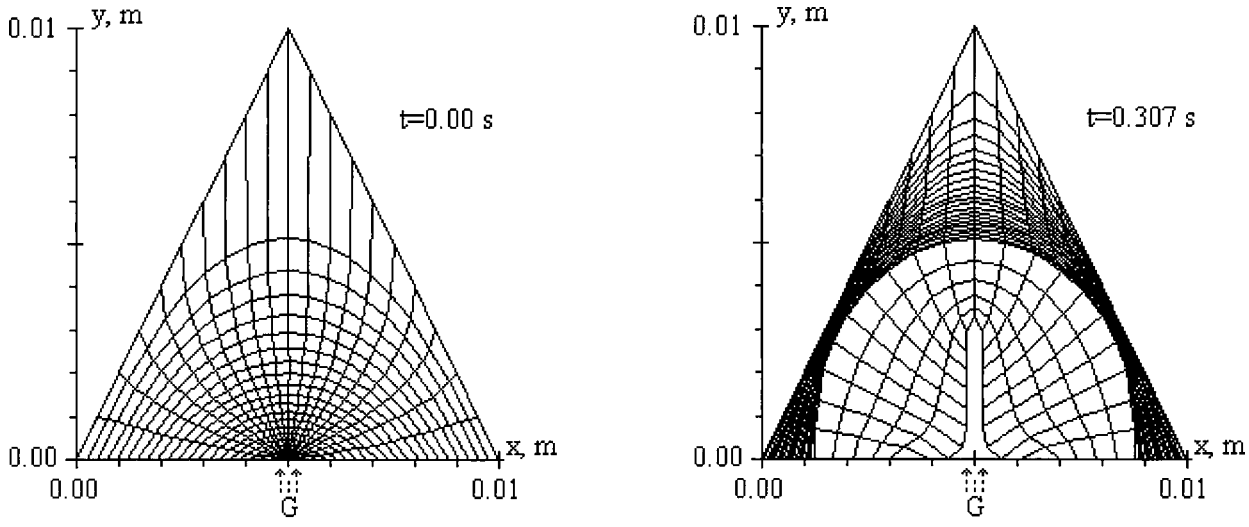

Figure 4. Computational grid in the physical space

At the second stage, which begins when the equilibrium melting temperature $T_m = 933.3°$ K is reached on the surface, the processes are described by the two-phase Stefan model. To introduce a new (liquid) phase, overheating of the irradiated surface by 0.1° K is provided. From the relation of the overheating energy and the latent heat L_m the initial thickness of the liquid phase is determined (about 10^{-8} m) and a new subregion Ω_l, $\Omega_{xy} = \Omega_s \cup \Omega_l$ is introduced. The computational grid with 21×6 nodes is located in the new phase (the total number of nodes is 21×26). From this moment the grid is reconstructed on each time layer. The numerical solution is accompanied by a radical reorganization of the computational grid (Fig. 4). Fragments of the physical space immediately after the new phase introduction are shown in Fig. 5 on an expanded scale.

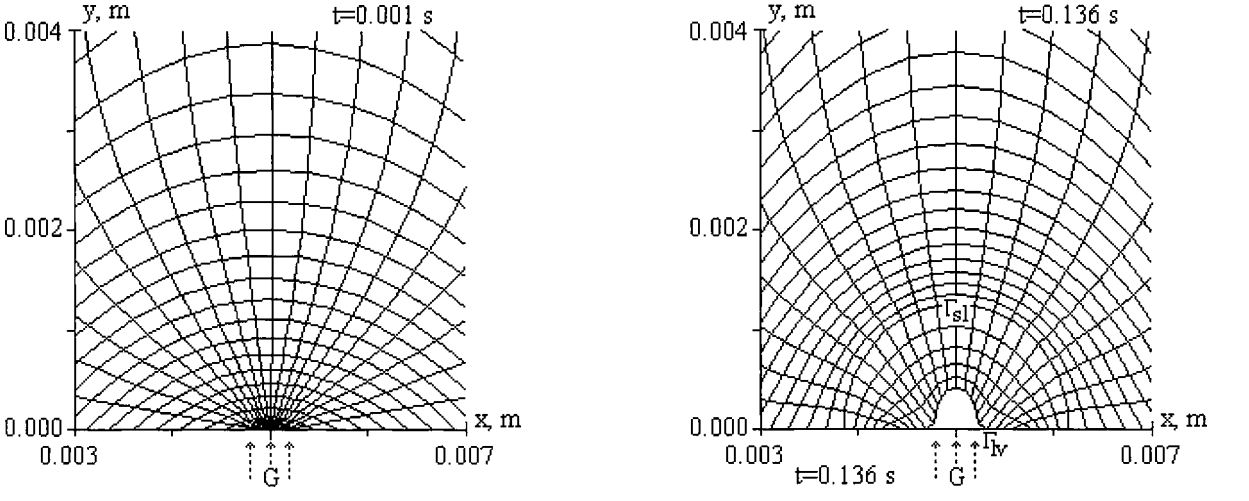

Figure 5. Physical space fragments with introduced liquid phase

The features of the problem are a high velocity of interfaces and a considerable deformation of the initial area. The changes in the maximum temperature in Ω_{xy} and maximum velocities of interface boundaries Γ_{sl} and Γ_{lv} are presented in Fig. 6.

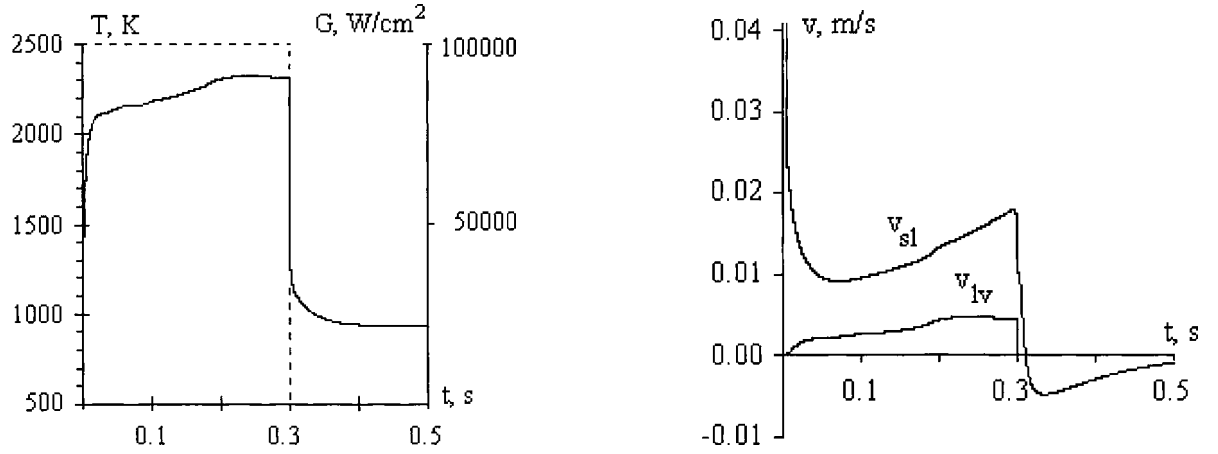

Figure 6. Change in the maximum temperature and maximum velocities

The maximum velocity v_{sl} reaches $\sim$1 m/s immediately after the introduction of the liquid phase and then decreases to $\sim$0.015 m/s. The spatial profiles of temperature fields in the region Ω_{xy} and the location of the phase interface Γ_{sl} (the isoline $T = 933.3°$ K) at different moments are given in Fig. 7–8. Two of them (Fig. 7) correspond to the influence of the source on the target ($G = 10^5$ W/cm^2) and the other two (Fig. 8) correspond to its absence ($G = 0$ W/cm^2). The processes of melting and evaporation lead to the formation of a deep channel in the zone of the influence and almost complete melting of the target. Cessation of the pulse leads to a sharp interruption of evaporation while the melting process continues for a longer time due to the large amount of energy stored in the liquid phase.

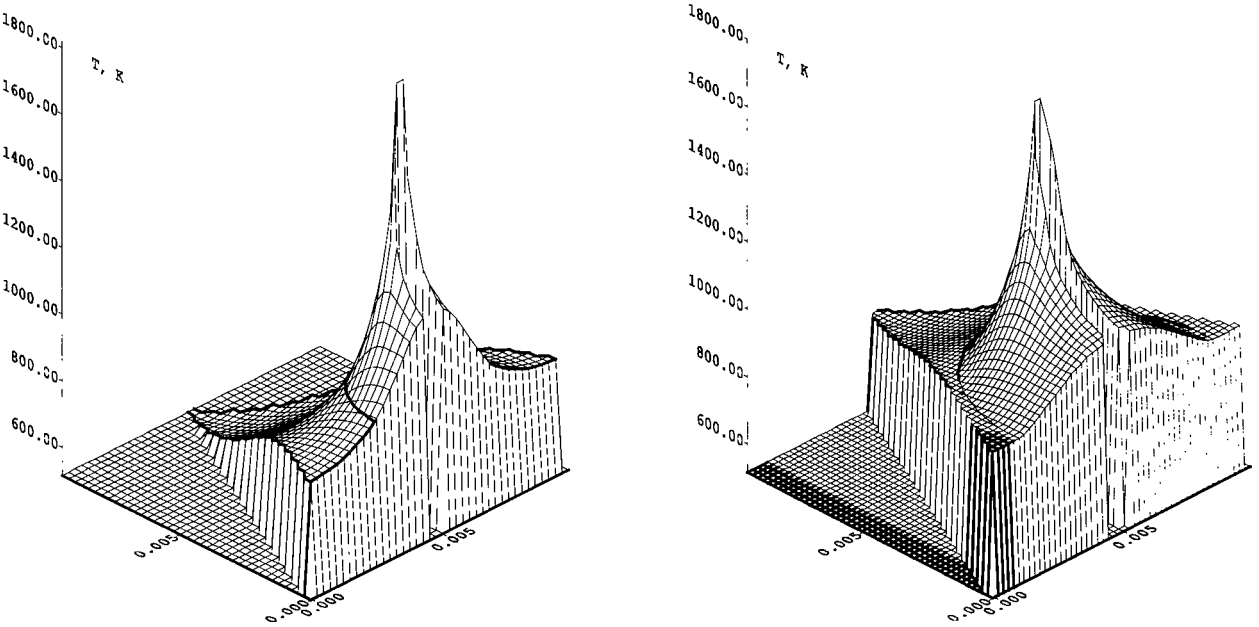

Figure 7. Spatial profiles for the temperature fields in the region Ω_{xy} for $t_1 = 0.01$ s and $t_2 = 0.24$ s respectively

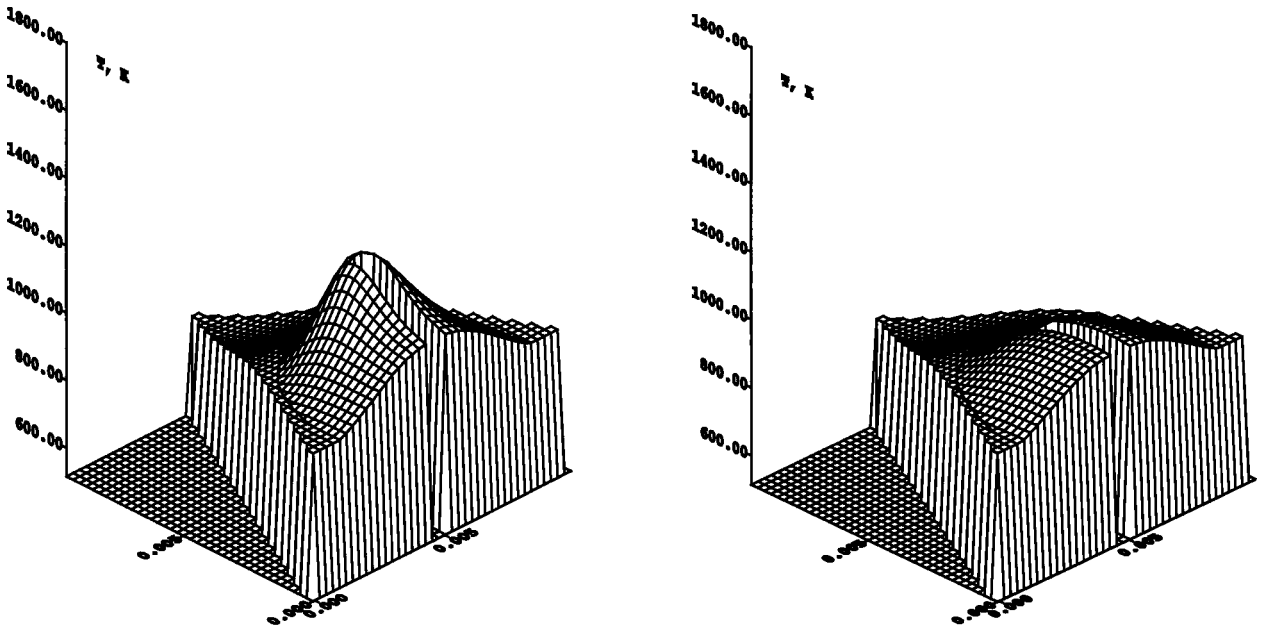

Figure 8. Spatial profiles for the temperature fields in the region Ω_{xy} for $t_3 = 0.31$ s and $t_4 = 0.32$ s respectively

The computing experiment shows a high efficiency of the method of dynamic adaptation for the considered problems of material processing.

References

[1] P. Brerslavsky and V. Mazhukin, *Mathematical modeling og processes of metal pulse melting and evaporation with explicit front-tracking*, Inzh. Fiz. Zh, **57** (1989), No. 1, pp. 107–114, in Russian.

[2] N. Dar'in and V. Mazhukin, *One approach to adaptive grid generation*, Docl. Akad. Nauk SSSR, **298** (1988), No. 1, pp. 64–68, in Russian.

[3] M. Davis, P. Kapadia, and J. Dowden, *The numerical solution of Stefan problems with front tracking and smoothing methods*, J. Comput. Phys., **60** (1985), pp. 534–548.

[4] W. W. Duley, *Laser processing and analysis of materials*, Plenum Press, New York an London, 1983, in Russian.

[5] V. Mazhukin, P. Prudkowskii, and A. Samokhin, *Entropy variation on the evaporation front*, Mat. Modellirovanie, **6** (1994), No. 11, pp. 3–10, in Russian.

[6] G. H. Meyer, *The numerical solution of Stefan problems with front tracking and smoothing methods*, Appl. Math. Comput, **4** (1978), pp. 283–306.

[7] N. Rykalin, A. Uglov, I. Zuev, and A. Kokora, *Laser and electron-beam processing of materials*, Mashinostroenie, Moscow, 1985, in Russian.

[8] A. Samarskii and V. Mazhukin, *Mathematical moddeling in the technology of laser treatments of material*, Surv. Math. Industry, **4** (1994), No. 1, pp. 85–149.

[9] A. Samarskii, V. Mazhukin, and M. Chuiko, *Dynamic adaptation method for non-stationary multidimensional Stefan problems*, Doclady RAS, **368** (1999), No. 3, pp. 307–310, in Russian.

[10] A. Samarskii and G. Moiseenko, *Effective homogeneous scheme for multidimensional Stefan problem*, Zh. Vychisl. Mat. Mat. Fiz., **5** (1965), No. 5, pp. 816–827, in Russian.

[11] A. A. Samarskii, *The Theory of Difference Schemes*, Marcel Dekker, Inc., New York — Basel, 2001.

[12] G. Shneider and M. Zedan, *A modified strongly implicit procedure for the numerical solution of field problems*, Numer. Heat Transfer, **4** (1981), No. 1, pp. 1–19.

[13] J. F. Thompson, Z. U. A. Warsi, and C. W. Mastin, *Boundary fitted coordinate systems for numerical solution of partial differential equations. - a review*, J.Comput.Phys., **47** (1982), No. 1, pp. 1–108.

Received 15 May 2002
Revised 21 Oct. 2002